THE JOURNAL OF PHYSICAL CHEMISTRY C

ARTICLE

pubs.acs.org/JPCC

Anisotropy and Transport Properties of Tubular C-BN Janus Nanostructures

M. M. Wu,[†,‡,#] X. Zhong,[§,#] Q. Wang,[∥,‡] Q. Sun,[*,†,∥,‡] R. Pandey,[§] and P. Jena[‡]

[†]Department of Materials Science and Engineering, Peking University, Beijing 100871, People's Republic of China

[‡]Department of Physics, Virginia Commonwealth University, Richmond, Virginia 23284, United States

[§]Department of Physics, Michigan Technological University, Houghton, Michigan 49931, United States

[∥]Center for Applied Physics and Technology, Peking University, Beijing 100871, People's Republic of China

ABSTRACT: By use of density functional theory and nonequilibrium Green's function technique we have studied the electronic structure and transport properties of tubular Janus structures composed of hybridized carbon (C) and boron-nitride (BN) nanotubes (NTs) with carbon caps at both ends. The effect of chirality was probed by focusing on (5, 5) armchair and (9, 0) zigzag structures, both of which have similar radii and are metallic in the infinite length limit. The study has revealed a number of interesting properties: (1) The highest-occupied molecular orbital (HOMO)−lowest-unoccupied molecular orbtial (LUMO) gap is decreased when BN patch is inserted to zigzag structure but increased when it is inserted in the arm chair structure and graphene sheet. (2) The zigzag edges of the heterojunctions lead to anisotropy of frontier orbital distribution where the HOMO and LUMO are respectively predominated by B−C and N−C bonding states. Consequently, one side or one end becomes more reactive than the other. (3) The current in tubular Janus structures is reduced from that in pristine carbon nanotubes. At low bias, the current in the zigzag structure increases with increasing tube length while reverse is the case with the arm chair structure.

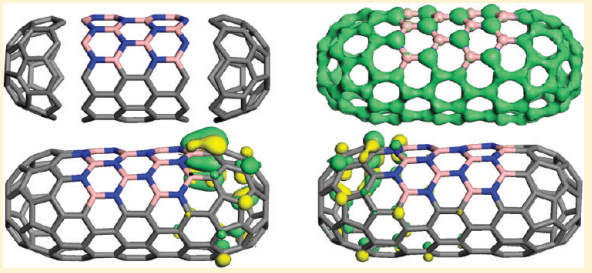

I. INTRODUCTION

Design and synthesis of multifunctional nanoparticles are topics of great current interest due to their versatility in technological applications. One of the early ways to synthesize these structures was to put two hemispherical particles, with different chemical composition and functionality, together. These particles have been referred to as Janus particles, a term coined by De Gennes[1] in 1992. The term Janus particle was named after the Roman god Janus who is characterized as having two heads, one looking at the past and the other looking into the future, i.e., the god Janus could perform two operations simultaneously. With the advances in shape-controlled synthesis, the Janus structures are now extended from a dotlike to rodlike and disklike[2] shapes. Several techniques and strategies,[3−9] such as electrochemical and photochemical reduction, templating of porous membranes and nanotubes, and surfactant-aided growth, have been developed for the fabrication of diverse Janus structures. The anisotropies in shape, size, and compositions of these particles provide flexible variables to tune the functions for applications in biomedicine, sensors, catalysis, photovoltaic device for light harvesting, and assembled porous materials for controlled gas storage and release.

In this paper, we study the tubular C-BN Janus structures which are motivated by recent experimental and theoretical advances in BN and C nanostructures. We note that the lattice mismatch plays an important role in the synthesis of hybrid structures composed of different chemical components. We chose to integrate C and BN nanotubes in forming Janus nanostructures since BN and C−C are isoelectronic and possess similar structures. For example, benzene (C_6H_6) and borazine ($B_3N_3H_6$), graphene and BN sheets, C-nanotube and BN-nanotube exhibit similar structures even though the physical and chemical properties of carbon and its BN counterpart are quite different. For example, C_6H_6 is aromatic, while $B_3N_3H_6$ is nonaromatic; a graphene sheet is metallic-like, while a BN sheet is a wide-gap semiconductor, and carbon nanotube can either be metallic or semiconducting depending on its chirality, while all BN nanotubes are semiconducting. These similarities and dissimilarities have stimulated considerable interest in C-BN hybrid structures, since the similarities in geometry guarantee a match in the lattice and bond length, while the dissimilarities in properties provide the diversity and tenability of the functions and performance. In fact, carbon−boron−nitride (C/BN) single-walled nanotubes (SWNTs) have been directly synthesized by bias-assisted hot filament chemical vapor deposition (CVD),[10] and SWNTs containing BN nanodomains were also fabricated by laser vaporization.[11] Recently a two-dimensional C/BN hybrid atomic sheet has been synthesized through thermal catalytic CVD method.[12] Here all the B and N atoms form BN pairs with each other, giving rise to domains. By controlling the shape and size of BN domains unexpected electronic and magnetic properties can emerge.

Received: August 18, 2011
Revised: October 27, 2011
Published: November 15, 2011

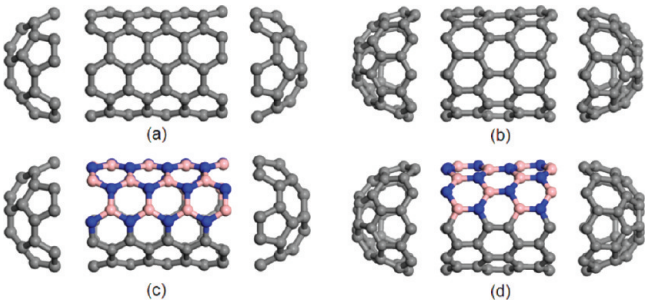

Figure 1. Schematic geometries of finite capped tubes for pristine (5,5) (a), pristine (9,0) (b), Janus (5,5) (c), and Janus (9,0) (d).

For example, the electronic band structure can be tuned from a direct gap to an indirect gap, and the energy gap can be further modulated by changing the bonding patterns. Theoretically, a strong tendency for BN hexagon formation has been found when B and N are introduced to C nanotubes.[13] This confirmed the experimental observation of the formation of BN nanodomains in carbon nanotubes. Furthermore, calculations based on density functional theory have been performed on infinite one-dimension Janus $C_{0.5}(BN)_{0.5}$ SWNTs.[14] The results suggest that the Janus type structures are dynamically stable, and the electronic structures are dependent on the chirality. For example, when going from pristine C-(m, m) to Janus $C_{0.5}(BN)_{0.5}$-(m, m) with m = 6, 10, and 16, the systems display negligible band gaps around the Fermi level.[14] For zigzag tubes the situation is different. While the pristine C(12,0) is metallic, the Janus $C_{0.5}$-$(BN)_{0.5}$(12,0) becomes semiconducting with a gap of 0.774 eV, similar to what happens for the band gap opening when BN domains are embedded in a graphene sheet. The existing studies indicate that the effect of BN insertion in controlling band gaps is much less effective in metallic arm-chair carbon nanotube than that of metallic zigzag carbon nanotube. This shows the diversity and complexity that chirality of nanotubes offer compared to that of two-dimensional graphene sheets.

To further increase the diversity of nanostructures, we explore the effect limiting the length of nanotubes and capping both the ends. Compared to infinite tubes, besides chirality and tube radius, additional variables can be introduced. In infinite tube, the heterojunctions of ...N−B−N−C−C... and ...B−N−B−C−C... are along the tube axis having zigzag configuration (for arm chair tube) or armchair configuration (for zigzag tube). For a finite capped tube, we have two additional junctions with two caps, which would make additional contributions to the interface effect. Moreover, the tube length also provides an additional degree of freedom. In this study, we investigate finite Janus $C_{0.5}(BN)_{0.5}$ SWNTs focusing on (5,5) armchair and (9,0) zigzag structures. Since both have very similar radii but different chiralities, we can probe the effect of chirality alone. Meanwhile, the radius of C_{60} is very close to those of (5,5) and (9,0), so it can be used as caps for the two ends of the tube[15] (see Figure 1). We also varied the tube length in the range 1.7 to 2.6 nm. The (5,5) structures contain 140 and 200 atoms, and the (9,0) structure contains 150 and 222 atoms, respectively.

II. COMPUTATIONAL METHODS

Our calculations were based on density functional theory (DFT) with generalized gradient approximation (GGA) for the exchange-correlation energy. We have used the Perdew−Wang 91 form[16] for the GGA and a plane-wave basis set with the projector-augmented-wave (PAW) method originally developed by Blochl[17] and adapted by Kresse and Joubert in the Vienna ab initio simulation package (VASP).[18] The structure optimizations were carried out using a conjugate−gradient algorithm without symmetry restriction. The convergence for the energy and the force was set to 0.0001 eV and 0.01 eV/Å, respectively. The energy cutoff was set to 280 eV. We used a supercell approach with 15 Å of vacuum space along the x, y, and z directions. Because of the large supercell, the Γ point was used to represent the Brillouin zone.

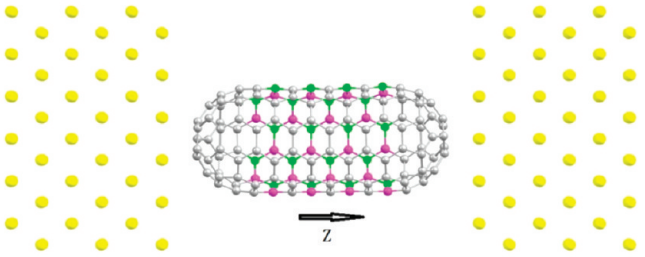

Figure 2. A schematic illustration of the Au-hybrid CNT-Au device. (Au in gold, C in gray, B in purple, and N in green).

For the calculations of electronic transport properties, we consider the following models: The capped nanotubes are sandwiched between two gold leads with a contact distance of 2.4 Å (Figure 2). These tubes end with pentagons (140 and 200 atom-tubes) or hexagons (150 and 222 atom-tubes) whose center points toward the center of one square of gold layer on the left side. The orientation of the contact surface was chosen in such a way that one side of pentagon or hexagon is parallel to one side of gold square. As a bias is applied on both sides of gold contact, the corresponding current is calculated using density functional theory coupled with nonequilibrium Green's function (NEGF).

The current is calculated using the formula

$$I = \frac{e}{h}\int_{-\infty}^{\infty} \det(E,V)[f(E-\mu_1) - f(E-\mu_2)]$$

where μ_1 and μ_2 are the electrochemical potentials in the two contacts under an external bias V, $f(E)$ is the Fermi−Dirac distribution function, and T is the transmission function. At the low temperature limit, $f(E)$ is a step function. This formula can be simplified to (at zero Kelvin)

$$I = \frac{e}{h}\int_{-V/2}^{V/2} \det(E,V)$$

since $V = \mu_1 - \mu_2$. Thus, the transmission function integral within corresponding bias window $(-V/2, V/2)$ determines the value of current.

III. RESULTS AND DISCUSSION

1. (5,5) Armchair Pristine and Hybrid Structures. We first study the (5, 5) armchair structures, where the two caps at the two ends are halves of C_{60} with armchair edges.[15] In the pristine C structures containing a total of 140 and 200 C atoms, the tube part contains 80 and 140 C atoms, respectively. In the Janus structures, the tube parts consist of $B_{20}N_{20}C_{40}$ and $B_{35}N_{35}C_{70}$. These are equivalent to heterojunctions between two curved BN ribbons and two curved graphene ribbons. The finite Janus structures are different from those with infinite length.[14] In these cases the structures contain heteroarmchair junctions with the

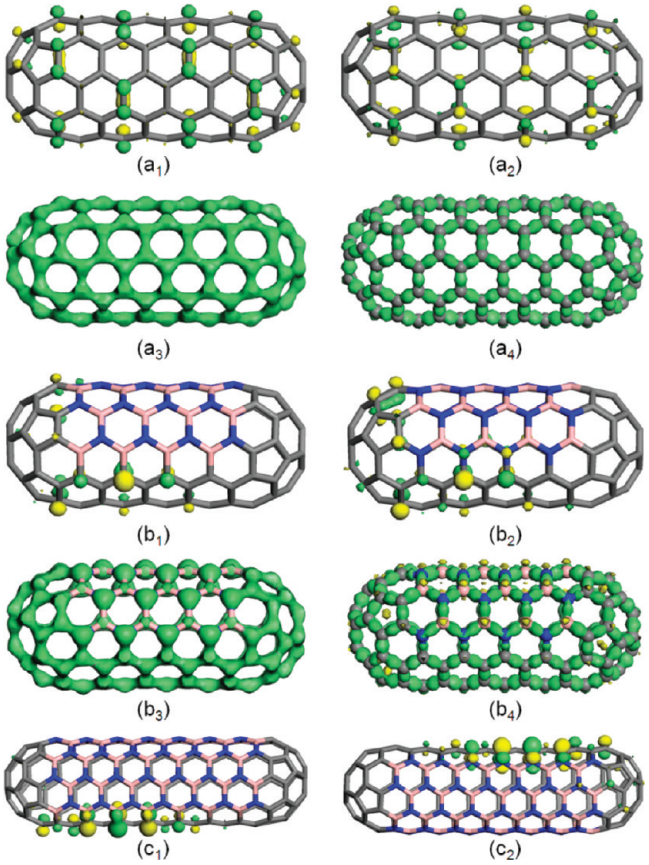

Figure 3. HOMO (a_1), LUMO (a_2), total charge density (a_3), and difference charge density (a_4) for structure C_{30}-C_{80}-C_{30}. The corresponding plots for C_{30}-$B_{20}N_{20}C_{40}$-C_{30} are given (b_1), (b_2), (b_3), and (b_4), respectively. Note that in b_2 the tube is rotated 180° compared with b_1 to show the localization of the LUMO. The isosurface value is 0.025 for the HOMO and LUMO orbitals, 1.5 for the total densities, and 0.15 for the difference charge density. (c_1) and (c_2) are the HOMO and LUMO for C_{30}-$B_{35}N_{35}C_{70}$-C_{30}.

caps and the heterozigzag junctions along the tube axis. Structure optimizations indicate that the pristine and the hybrid structures are very similar in geometries due to near perfect match in the bond lengths between B−N and C−C. However, their electronic structures are different because of the different electronic configurations and different electronegativities of C, B, and N. C has one electron more than B but one electron less than N. Hence, the electronegativity of C is also between those of B and N.

For comparison we first discuss the pristine structure with 140 atoms. The calculated energy gap between highest-occupied molecular orbital (HOMO) and lowest-unoccupied molecular orbital (LUMO) is 0.43 eV. The frontier orbitals of HOMO, LUMO, total charge density, and difference charge density are given in Figure 3, parts a_1−a_4, respectively. We can see that the HOMO is more homogeneously distributed than LUMO and the sp^2 covalent bonding features are well reproduced in the difference charge density (Figure 3a_4). When 40 C atoms in the tube part are replaced with $B_{20}N_{20}$, a hybrid structure of C_{30}-$B_{20}N_{20}C_{40}$-C_{30} is formed. The energy gap is increased to 0.60 eV due to the enhanced electron localizations when BN is introduced. The corresponding frontier orbitals and charge density are shown in Figure 3, parts b_1−b_4. The induced anisotropies can be clearly seen. We note that the 2D hexagonal lattice of boron

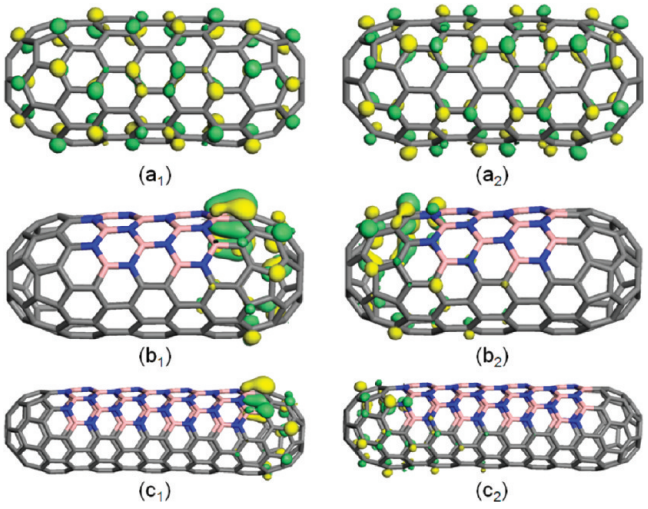

Figure 4. (a_1), (b_1), and (c_1) are the HOMOs for C_{39}−C_{72}−C_{39}, C_{39}−$B_{18}N_{18}C_{36}$−C_{39}, and C_{39}−$B_{36}N_{36}C_{72}$−C_{39}; the corresponding LUMOs are (a_2), (b_2) and (c_2).

nitride consists of two inequivalent sublattices. Thus, in the $B_{20}N_{20}$ nanoribbon the two zigzag edges parallel to the tube axis are inequivalent. One edge links with C atoms through N sites and the other edge through B sites. This affects the frontier orbital distributions. For example, the HOMO is mainly on C sites linked with B along the zigzag junction, while the LUMO is mainly on C sites linked with N along the zigzag junction. Moreover, charge transfers occur from B to N, B to C, and C to N due to the differences in their respective electronegativities. In this case the hybrid structure has hybrid bonding features, namely, mixed covalent and ionic bondings.

Next we change the tube length to study its effect on the induced anisotropy. We extend the structures from C_{30}-C_{80}-C_{30} and C_{30}-$B_{20}N_{20}C_{40}$-C_{30} to C_{30}-C_{140}-C_{30} and C_{30}-$B_{35}N_{35}C_{70}$-C_{30}. We find that for the C_{30}-C_{140}-C_{30} structure, the main features of frontier orbitals and charge density distributions are very similar to those of C_{30}-C_{80}-C_{30}. The HOMO−LUMO gap is slightly reduced to 0.42 eV. For the hybrid structures, as the ratio of BN pairs to C atoms goes from 20 to 26%, the induced anisotropies are enhanced. These are shown in parts c_1 and c_2 of Figure 3 for the HOMO and LUMO, where the main contributions are from zigzag edges with B−C bonding on one side or N−C bonding on the other side.

2. (9,0) Zigzag Pristine and Hybrid Structures. Following the same procedure as outlined in the above, we studied the finite (9, 0) zigzag structures including C_{39}−C_{72}−C_{39}, C_{39}−$B_{18}N_{18}C_{36}$−C_{39}, C_{39}−C_{144}−C_{39}, and C_{39}−$B_{36}N_{36}C_{72}$−C_{39}. Here the two ends of the tube are capped with 39 atoms cut from C_{60} with zigzag edges, which are connected with the tube. In Figure 4, the HOMO and LUMO are plotted for C_{39}−C_{72}−C_{39}, C_{39}−$B_{18}N_{18}C_{36}$−C_{39}, and C_{39}−$B_{36}N_{36}C_{72}$−C_{39}.We can see that for the pristine capped nanotube both HOMO and LUMO are homogeneously distributed except for the hexagons in the cap ends. However, the situations are very different for the hybrid structures. The HOMO is mainly on the end with BN zigzag edge bonding with carbon cap through B atoms, while the LUMO is on the other end with BN zigzag edge bonding with carbon cap through N atoms (see Figure 4 b_1 and b_2). These features remain for the longer tube, namely, C_{39}−$B_{36}N_{36}C_{72}$−C_{39}, as shown in parts c_1 and c_2 of Figure 4. In contrast to the results in the arm

chair structures, the induced anisotropies are mainly on the tube ends.

For the pristine structures of $C_{39}-C_{72}-C_{39}$ and $C_{39}-C_{144}-C_{39}$, the calculated HOMO−LUMO gaps are 0.79 and 0.26 eV, respectively. This suggests that the electrons become more delocalized and the metallicity gets enhanced as the tube length increases. However, as BN patch is introduced the gaps are reduced to 0.08 and 0.07 eV, respectively. This is very different from the results in arm chair structures and graphene sheet, indicating that the semiconducting BN patches not only can open or widen the gap but can also reduce the gap. Figure 5 shows a comparison of density of states (DOS) for the pristine and hybrid structures. We can see that when BN patch is inserted additional states appear in the gap of the pristine structure.

3. Electronic Transport Properties of the Pristine and Hybrid Structures. Next we study electronic transport property of the hybrid structures. The analysis shows that pristine 140 CNT can conduct the highest current (Figure 6a) relative to other pristine CNTs. The magnitude of current appears to follow the band gap in the small bias range (0−0.3 V): 222 CNT has the smallest HOMO−LUMO gap, while the 150 tube has the largest gap, and gaps in 140 and 200 CNTs lie in between. The values of the HOMO−LUMO gaps are in agreement with the previously reported results.[19,20] We note as the bias value is increased from 0.3 to 1.0 V, the armchair CNTs are carrying larger current than the zigzag ones with 140 CNT having the highest current and 150 CNT having the smallest value.

The hybrid C/BN-NTs are found to exhibit similar $I-V$ characteristics (Figure 6b). For the bias ranging from 0 to 1 V, 140 tube gives the largest current while 150 tube gives the smallest current. 222 tube shows a negative differential resistance at around 0.2 V, but the current monotonically increases above the bias value of 0.4 V.

Compared with pristine CNT counterparts, all hybrid C/BN-NTs exhibit reduced electron conduction. This is what we expected since hybrid C/BN-NTs should have properties which are in between those exhibited by CNT and BN-NT. Note that BN and carbon both contribute to one-half of primitive cells and tubular configuration of BN is relatively a good insulator. The electron conductivity of a hybrid $C_x(BN)_y$ nanotubes was also shown to be intermediate between carbon nanotubes (CNT) and BN nanotubes (BN-NT). In fact, the properties of current can be precisely explained by the underlying transmission functions. In Figure 7 we plot the transmission functions of 150 pristine CNT and hybrid C/BN-NT under zero bias as an example.

We also know that in general when the external bias is changed slightly, the corresponding transmission function would also change slightly,[21] so we can estimate the trend of the change of current at low bias. When the bias is increased, the bias window is also enlarged. Pristine CNT have higher peaks in most ranges except in the vicinity of E_f, so at higher bias it should exhibit higher current than hybrid C/BN-NT.

Local density of states can also explain the decrease of current in hybrid C/BN-NT, see Figure 8. As mentioned above, hybrid C/BN-NT is intermediate between pristine CNT and BN-NT. At low bias, the conducting properties are dominated by electrons with energies close to E_f. Figure 8 clearly shows the deficiency of electrons in the BN region of hybrid C/BN-NT in an energy range close to E_f, leading to a suppression of conduction channels, resulting in a smaller current.

It is worthy to note the limitation of LDA/GGA-DFT level of theory in estimating the band gaps of carbon nanostructures.

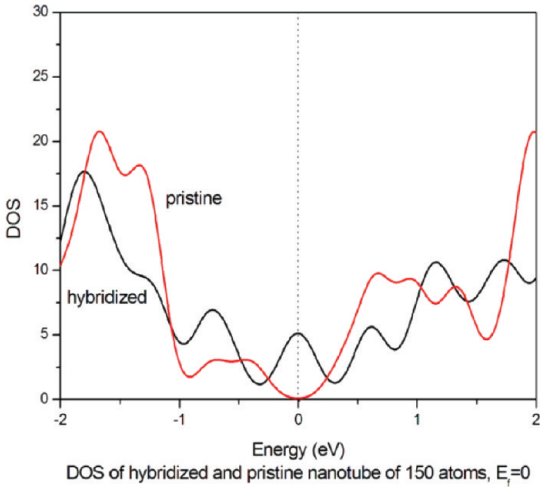

Figure 5. Density of states of pristine $C_{39}-C_{72}-C_{39}$ and hybrid $C_{39}-B_{18}N_{18}C_{36}-C_{39}$.

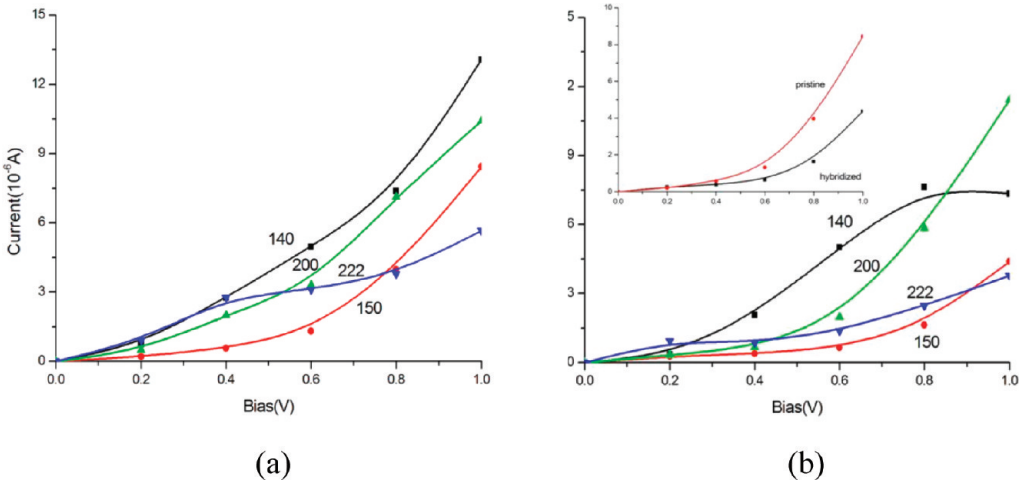

Figure 6. $I-V$ curves of pristine CNTs (a) and hybrid C/BN-NTs (b). Insert: comparison of 150 pristine CNT and hybrid C/BN-NT.

dx.doi.org/10.1021/jp207973b |J. Phys. Chem. C 2011, 115, 23978–23983

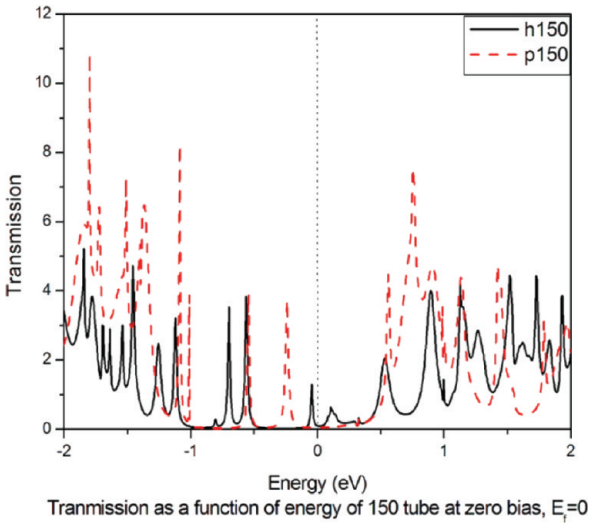

Figure 7. Transmission functions of 150 pristine CNT and hybrid C/BN-NT with gold contacts at zero bias.

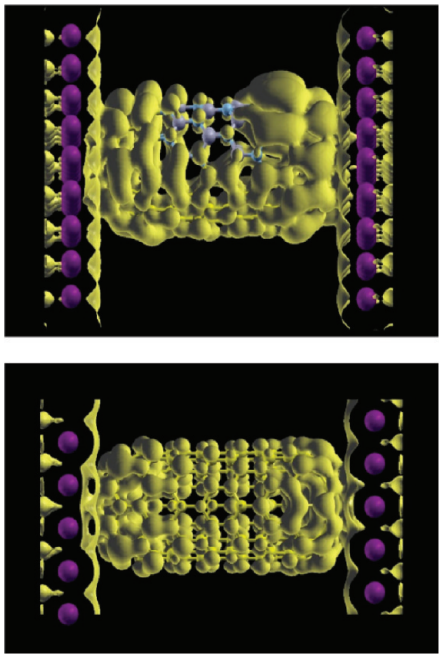

Figure 8. LDOS of 150 nanotubes within energy range $E_f \pm 0.1$ V. Upper: hybrid C/BN-NT. Lower: pristine CNT.

A qualitative trend in transport properties is, however, not expected to be different if one employs hybrid functionals to perform the transport calculations. This is because the transport properties of a C-BN based device systems are indirectly related to their band gaps.

IV. SUMMARY

First-principles theoretical studies reveal that Janus nanostructures can be created by grafting BN and C nanotubes together. The functionality of these structures can be tuned by changing the tube length and the tube radius as well as by changing their chirality and capping the open ends. We note that, while BN and C−C are isoelectronic and BN- and C-based structures show similar geometrical arrangements, their electronic properties are very different. Thus integrating BN into C nanostructures provides avenues for the design of anisotropic particles. We demonstrate this by calculating in detail frontier orbitals, charge distributions, and electron transport. Compared to the pristine structures and infinite tubes, we find that the finite hybrid tubular Janus structures provide opportunities to modulate their properties by controlling their size, composition, and synthesis. The zigzag heterojunctions induce strong anisotropy in frontier orbital distribution, which result in anisotropic reactions. The HOMO−LUMO gaps and electric current can be enhanced or reduced either by changing the tube length or by inserting BN patch. Our study clearly suggests that hybridizing C and BN would be an effective pathway to fabricate diverse nanostructures with exotic physical and chemical properties.

AUTHOR INFORMATION

Corresponding Author

*E-mail: sunqiang@pku.edu.cn.

Author Contributions

#The first two authors contributed equally to this work.

ACKNOWLEDGMENT

This work is partially supported by grants from the National Natural Science Foundation of China (Grant Nos. NSFC-10874007 and NSFC-21173007), the China Scholarship Council, and the U.S. Department of Energy. This research used resources of the National Energy Research Scientific Computing Center, which is supported by the Office of Science of the U.S. Department of Energy under Contract No. DE-AC02-05CH11231.

REFERENCES

(1) De Gennes, P. D. *Rev. Mod. Phys.* **1992**, *64*, 645.
(2) Walther, A.; Drechsler, M.; Rosenfeldt, S.; Harnau, L.; Ballauff, M.; Abetz, V.; Muller, A. H. E. *J. Am. Chem. Soc.* **2009**, *131*, 4720.
(3) Glotzer, S. C. *Science* **2004**, *306*, 419.
(4) Nie, Z. H.; Li, W.; Seo, M.; Xu, S. Q.; Kumacheva, E. *J. Am. Chem. Soc.* **2006**, *128*, 9408.
(5) Nisisako, T.; Torii, T.; Takahashi, T.; Takizawa, Y. *Adv. Mater.* **2006**, *18*, 1152.
(6) Nisisako, T.; Torii, T. *Adv. Mater.* **2007**, *19*, 1489.
(7) Paunov, V. N.; Cayre, O. *J. Adv. Mater.* **2004**, *16*, 788.
(8) Perro, A.; Reculusa, S.; Ravaine, S.; Bourgeat-Lami, E. B.; Duguet, E. J. *Mater. Chem.* **2005**, *15*, 3745.
(9) Walther, A.; Andre, X.; Drechsler, M.; Abetz, V.; Muller, A. H. E. *J. Am. Chem. Soc.* **2007**, *129*, 6187.
(10) Wang, W. L.; Bai, X. D.; Liu, K. H.; Xu, Z.; Golberg, D.; Bando, Y.; Wang, E. G. *J. Am. Chem. Soc.* **2006**, *128*, 6530.
(11) Enouz, S.; Stephan, O.; Cochon, J. L.; Colliex, C.; Loiseau, A. *Nano Lett.* **2007**, *7*, 1856.
(12) Ci, L.; Song, L.; Jin, C. H.; Jariwala, D.; Wu, D. X.; Li, Y. J.; Srivastava, A.; Wang, Z. F.; Storr, K.; Balicas, L.; Liu, F; Ajayan, P. M. *Nat. Mater.* **2010**, *9*, 430.
(13) Ivanovskaya, V. V.; Zobelli, A.; Stephan, O.; Briddon, P. R.; Colliex, C. *J. Phys. Chem. C* **2009**, *113*, 16603.
(14) Du, A. J.; Chen, Y.; Zhu, Z. H.; Lu, G. Q.; Smitht, S. C. *J. Am. Chem. Soc.* **2009**, *131*, 1682.
(15) Saito, R.; Fujita, M.; Dresselhaus, G.; Dresselhaus, M. S. *Appl. Phys. Lett.* **1992**, *2204*, 60.
(16) Wang, Y.; Perdew, J. P. *Phys. Rev. B* **1991**, *44*, 13298.
(17) Blochl, P. E. *Phys. Rev. B* **1994**, *50*, 17953.

(18) Kresse, G.; Joubert, D. *Phys. Rev. B* **1999**, *59*, 1758.
(19) Gan, L. H.; Zhao, J. Q. *Physica E* **2009**, *41*, 1249.
(20) Cioslowski, J.; Rao, N.; Moncrieff, D. J. *Am. Chem. Soc.* **2002**, *124*, 8485.
(21) Zhong, X.; Pandey, R.; Rocha, A. R.; Karna, S. P. *J. Phys. Chem. Lett.* **2010**, *1*, 1584.